Finite-element simulation models and experimental verification for through-silicon-via etching: Bosch process and single-step etching

Zihao Ouyang, Wenyu Xu, D. N. Ruzic, Mark Kiehlbauch, Alex Schrinsky, and Kevin Torek

Citation: Journal of Vacuum Science & Technology A **32**, 041303 (2014); doi: 10.1116/1.4882215
View online: http://dx.doi.org/10.1116/1.4882215
View Table of Contents: http://scitation.aip.org/content/avs/journal/jvsta/32/4?ver=pdfcov
Published by the AVS: Science & Technology of Materials, Interfaces, and Processing

Articles you may be interested in
Etching mechanism of the single-step through-silicon-via dry etch using SF6/C4F8 chemistry
J. Vac. Sci. Technol. A **32**, 041306 (2014); 10.1116/1.4885500

Applying x-ray microscopy and finite element modeling to identify the mechanism of stress-assisted void growth in through-silicon vias
J. Appl. Phys. **110**, 053502 (2011); 10.1063/1.3629988

High rate deep Si etching for through-silicon via applications
J. Vac. Sci. Technol. A **29**, 021009 (2011); 10.1116/1.3543635

Atomic-scale cellular model and profile simulation of poly-Si gate etching in high-density chlorine-based plasmas: Effects of passivation layer formation on evolution of feature profiles
J. Vac. Sci. Technol. B **26**, 1425 (2008); 10.1116/1.2958240

Modeling of fluorine-based high-density plasma etching of anisotropic silicon trenches with oxygen sidewall passivation
J. Appl. Phys. **94**, 6311 (2003); 10.1063/1.1621713

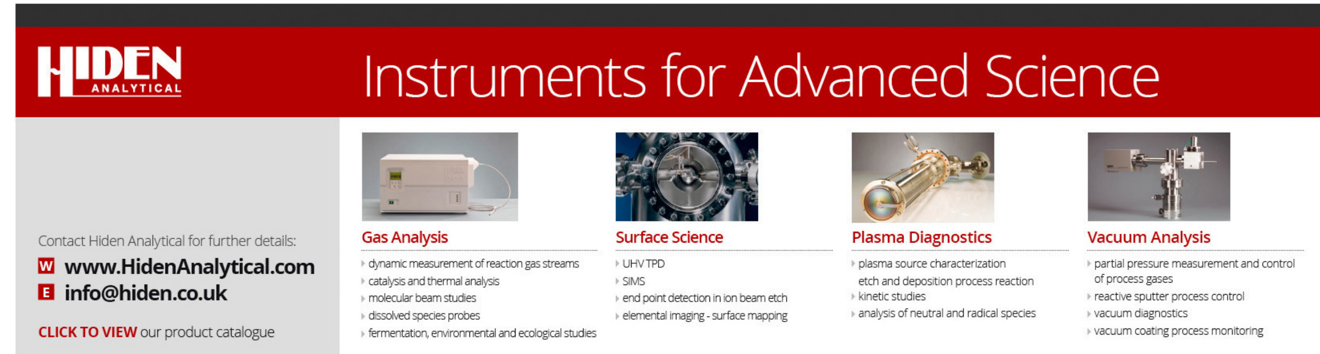

Redistribution subject to AVS license or copyright; see http://scitation.aip.org/termsconditions. Download to IP: 128.174.163.244 On: Mon, 11 Aug 2014 16:28:55

Finite-element simulation models and experimental verification for through-silicon-via etching: Bosch process and single-step etching

Zihao Ouyang,[a)] Wenyu Xu, and D. N. Ruzic
Center for Plasma Material Interactions, Department of Nuclear Plasma and Radiological Engineering, University of Illinois at Urbana-Champaign, Urbana, Illinois 61801

Mark Kiehlbauch, Alex Schrinsky, and Kevin Torek
Micron Technology, Inc., 8000 South Federal Way, Boise, Idaho 83707

(Received 20 February 2014; accepted 27 May 2014; published 10 June 2014)

In this study, time-dependent simulation models are established for both the Bosch process and single-step through-silicon-via (TSV) etching using SF_6 and C_4F_8 chemistry by employing a finite-element-method method. The simulation models take into account the thermal etching of F radicals, ion-enhanced etching, neutral deposition and ion-enhanced deposition mechanisms, as well as the angular dependence of the ion sputtering with aspect to a surface element. Comparison between the simulation results and experiments suggests that consideration of two ion fluxes (high-energy and low-energy) is critical for matching the simulation etch profile with the experiments. It is found that the underlying reason for the transition formed on the TSVs using the single-step etching originates from the difference of the ion angular distributions of etching species and depositing species. The Bosch process model successfully predicted profile details, such as the top scallops of the TSV profile, and the model established for single-step etching can be used to predict the transition position shown on the sidewalls. The simulation models can be used to study the individual effects of low-energy ions and the high-energy ions in the etching and passivation mechanisms for TSV etching in both Bosch process and single-step etching techniques. © *2014 American Vacuum Society*. [http://dx.doi.org/10.1116/1.4882215]

I. INTRODUCTION

Through-silicon-via (TSV) etching is an important process step for interconnecting function units and multiple logic, memory or sensor chips in a semiconductor device to obtain 3-D integration. TSVs usually have relatively large critical dimensions (CDs, 1–50 μm) with aspect ratios up to 15:1, depending on the specific integration scheme. High module density, low operation power and high bandwidth are the critical goals of using TSV technology in 3-D integrated devices. Depending on whether TSVs are fabricated before the initial process step, before metal filling, or after the final process step, etch processes are classified into "via-first," "via-middle," or "via-last," respectively.[1] Utilization of TSV techniques have the potential to become a critical approach to overcome the scaling limit in semiconductor industry. Applications using the TSV technique have been explored to realize higher bandwidth, higher density and lower power in semiconductor devices.

The dominating TSV etching technique in semiconductor industry to realize a high-aspect-ratio (HAR) profile with good sidewall passivation is known as the Bosch process.[2] In the Bosch process approach, F-based etching gas, such as SF_6, is commonly used as the etch gas to maximize etch rate (ER) during the etching step, and C_4F_8, C_4F_6, and CHF_3 are proved to be effective passivation gases to form polymers on sidewalls during the passivation step.[3,4] It is well-known that the key mechanism for the Bosch process to obtain anisotropic HAR structures is that the combination of physical ion sputtering and chemical etching in the etch step completely removes the passivation at the bottom of the features but only partially removes passivation on the sidewalls. Therefore, an optimal balance between etching and passivation is important for achieving good quality TSVs using the Bosch process: if polymerization is increased above the optimal balance, the time for the ions to punch though the passivation layer at the bottom increases to prevent further etching. However, polymerization below the optimal condition can lead to an isotropic etching due to insufficient passivation on the sidewalls.

Although the Bosch process is believed to have ability to achieve high ER and HAR, an intrinsic problem caused by this two-step alternating process is the sidewall scalloping defect. Scalloped profiles are highly undesirable because it can cause voids and defects in the subsequent metal filling processes, leading to physical and electrical failure on devices. A few single-step silicon etching processes have been studied to produce micro-sized trenches[5] and nanoscale pillars[6] using a combined SF_6/C_4F_8 chemistry. However, the remaining issues of these processes are low ER (0.22–1.6 μm/min[5,6]) and very low aspect ratio. The main reason for such low ERs may be related to the pairwise extinction effect due to mixture of etching and passivation gases.

Simulation work for TSV etching has potential for predicting TSV etching profiles by optimizing etching and passivation duration ratio in Bosch process and etching mechanisms in single-step etching. Simulation models established in this study are complemented by computational studies utilizing commercial program COMSOL Multiphysics (COMSOL, version

[a)]Electronic mail: ouyang2@illinois.edu

 0734-2101/2014/32(4)/041303/14/$30.00 © 2014 American Vacuum Society

Redistribution subject to AVS license or copyright; see http://scitation.aip.org/termsconditions. Download to IP: 128.174.163.244 On: Mon, 11 Aug 2014 16:28:55

4.3a). COMSOL uses the finite-element-method together with adaptive meshing to solve coupled multiphysics problems. Two important aspects in the model establishment need to be appropriately considered in order to simulate an etching process correctly: (1) Motions of each type of species participating in the etching process from a plasma. This includes interactions between particles due to collisions and interactions with an electromagnetic field if the particles are charged. For low pressure etching processes, collisions between particles in the TSV feature are negligible due to the fact that the mean free path of the particles is much larger than the feature size. (2) Surface reactions between the plasma species and the surface materials. This includes material removal, polymer deposition, and polymer sputtering induced by ions and neutrals.

Brief descriptions of models established for TSV etching using the Bosch process and single-step etching will be given in this paper, followed by considerations used in the simulation of TSV etching in a time-dependent manner. The variables used in the simulation model will be paired with the parameters of experiments, such as etching/passivation gas ratio, ion energy and ion angular distribution. Comparisons of etch profiles realized by simulation and experimental profile of the Bosch process and single-step etching will be discussed.

II. MODEL ESTABLISHMENT

A. Etching mechanism

In this study, the SF_6 etching is used in the Bosch process and is considered by the classic model proposed by Gerlach-Meyer.[7] Total ER consists of contributions from spontaneous (thermal) etching by neutral species, physical sputtering by ions, and ion-enhanced etching. In SF_6 plasmas, the thermal etching is mainly induced by fluorine atoms, and it can be characterized by the Arrhenius form

$$\mathrm{ER_{th}} = k_0 \exp\left(-\frac{E_a}{kT}\right)\Gamma_F, \tag{1}$$

where k_0 is the rate parameter, Γ_F is the atomic fluorine atoms, T is the substrate temperature, and E_a is the activation energy. The values of k_0 and E_a are chosen to be $3.59 \times 10^{-23}\,\mu\mathrm{m{\cdot}s{\cdot}m^2/min}$ and 0.108 eV.[8] The fluxes in this study are estimated by

$$\Gamma_i = \frac{P_i}{\sqrt{2\pi m_i k T_i}}, \tag{2}$$

where P_i is the partial pressure, m_i is the mass, and T_i is the temperature of species i.

The ERs of physical sputtering ($\mathrm{ER_{sp}}$) and ion enhanced etching ($\mathrm{ER_{ie}}$) are characterized by a model proposed by Gray *et al.*[9] and can be expressed as

$$\mathrm{ER_{sp}} = Y_{\mathrm{sp}}(1-\Theta_F)\Gamma_{\mathrm{ion}}, \tag{3}$$

$$\mathrm{ER_{ie}} = Y_{\mathrm{ie}}\Theta_F\Gamma_{\mathrm{ion}}, \tag{4}$$

where Y_{sp} and Y_{ie} are the yield of physical sputtering and ion-enhanced etching, Γ_{ion} is the ion flux, and Θ_F is the surface coverage fraction by fluorine atoms. Θ_F is determined by the fluorine surface sticking coefficient s on silicon

$$\Theta_F = \frac{s\left(\dfrac{\Gamma_F}{\Gamma_{\mathrm{ion}}}\right)}{s\left(\dfrac{\Gamma_F}{\Gamma_{\mathrm{ion}}}\right) + 2Y_{\mathrm{ie}}}. \tag{5}$$

Both Y_{sp} and Y_{ie} are found increase approximately with the square root of ion energy.[10] For fluorine plasmas,

$$Y_{\mathrm{sp}} = A\left(\sqrt{E_i} - \sqrt{E_{\mathrm{th}}}\right), \tag{6}$$

$$Y_{\mathrm{ie}} = B\sqrt{E_i}, \tag{7}$$

where E_{th} is the threshold energy with an order of magnitude of 10 eV.[11] Factors A and B are depending on the type of ion species and neutral-to-ion flux ratio. It is important to point out that Y_{sp} usually has a much smaller value than Y_{ie}. Data from Vitale *et al.*[12] has indicated that for an argon-enhanced F_2 plasma, E_{th} is around 50 eV, and the values of A and B are 0.022 and 2.35, respectively. This means the effect of sputtering is small enough to be ignored in the overall ER.

Mass spectroscopy analysis of the SF_6 plasmas has shown that SF_x^+ (x = 3 or 5) is the dominant positive ions and F atoms are the major neutral species.[13] The effect of silicon sputtering effect by SF_x^+ ions can be simulated by a Monte-Carlo simulator TRIDYN developed by Möller and Eckstein.[14,15] The ion-enhanced etching yield used in this study is estimated using the Ar-enhanced fluorine plasma data from Ref. 9. In the case of low-energy ions (20–200 eV), the silicon etching yield by Ar ions is in the range of 5–10 atom/ion and increases as neutral-to-ion ratio increases. The ion-enhanced silicon yield by SF_x^+ is expected to be larger than that of Ar ions due to possible dissociation of SF_x^+ ions into silicon lattice upon bombardment, and the released F can help to increase silicon ER. The effect of the SF_3^+ ion is considered in our simulation models, and its etching yield of Si can be set as a variable to investigate the effect of the reaction mechanism.

It is noticed that the ion–surface interaction is an extremely complicated process, especially when poly-atomic F-containing ions, such as SF_3^+, are involved. Since the energy of the chemical bond is usually much smaller than the bombardment energy, dissociation and neutralization processes should be expected upon ion bombardment, thus SF_3^+ ions can be dissociated and neutralized into multiple F or S atoms when they arrive at the silicon surface. The ratio and energy of the reflected ions strongly depend on ion incident angle (with respect to surface), ion energy, and ion mass. As an example, the number density ratio and energy ratio of the reflected F neutrals are calculated and shown in Fig. 1.

Considering a typical TSV profile, Fig. 1 indicates that for the bottom surfaces, where the ion incident angle is nearly 0 (with respect to surface normal), both the reflected

Redistribution subject to AVS license or copyright; see http://scitation.aip.org/termsconditions. Download to IP: 128.174.163.244 On: Mon, 11 Aug 2014 16:28:55

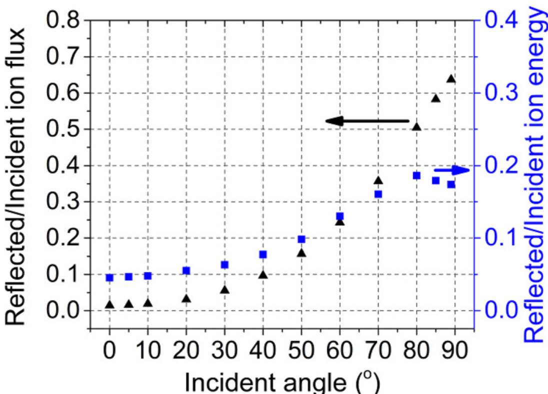

FIG. 1. (Color online) Energy and flux ratio of reflected F (incident ion energy: 30 eV).

density and energy is less than 1% of the incident ions. For the sidewall surfaces, although the reflection ratio is increased due to larger incident angle, the number density of ions (ion flux) is much smaller compared to that at the bottom surface; thus, the total etching contribution of reflected ions is also insignificant. On the other hand, reflected neutrals (mostly F atoms) will not affect etch profile significantly because it is assumed in the simulation model that the F neutrals are saturated in the ion-assisted etching term, which is the major contribution for etch profile. As a result, the reflected F neutrals only affect the thermal etching term, which is much smaller compared to the contribution of ion-assisted etching. Therefore, it can be assumed that the sticking coefficient of SF_3^+ ions is $\sim$1 in the simulation model.

B. Deposition mechanism

The passivation in C_4F_8 plasmas is made possible by the deposited fluorocarbon films formed by the decomposition of C_4F_8 molecules. Neutral CF_x radicals are critical for polymer formation on silicon surface. The morphology of deposited films is found to be strongly depending on the CF_x concentration.[16] Recombination reactions occur at a high rate when there is a high density of CF_x radicals, resulting in heavy fragment (C_xF_y) formation and powder/film deposition. At low densities of CF_x radicals, amorphous and cross-linked $(CF_x)_n$ films can be formed on silicon surface.

The deposition rate (DR) of the polymer resulted from neutral C_xF_y radicals can be related to the flux of these radicals Γ and their sticking coefficient s[17]

$$DR_{\text{neutral}} = \sum_i \frac{K_i}{\rho_{\text{film}}} \Gamma_i s_i, \tag{8}$$

where K_i is the number of carbon atoms incorporated into the film by neutral species i and ρ_{film} is the density of deposited film. Saraf *et al.*[17] estimated the upper bound of the largest possible sticking coefficient was only 0.15%. This indicates that neutral C_xF_y monomers are subject to frequent reflections by the feature walls before they are finally sticking to the growing film. Consequently, films grown solely by neutral fluorocarbon monomers should be close to conformal.

A study on the aspect ratio dependence of the deposition both at the bottom and on the sidewalls of trenches has showed that at the top of the sidewalls where undercut occurs has much lower film coverage than that at the bottom of the sidewalls.[17] This observation strongly implies that the ion-enhanced polymer deposition plays an important role in film growth for C_4F_8 plasmas. The mechanism for ion-enhanced deposition is probably similar to that for ion-enhanced etching. The ion bombardment creates reactive sites on silicon surface for neutral particles to attach, where the sticking coefficient increases substantially. If the flux of neutral species is much larger than the flux of the ions, the deposition rate of the polymer resulted from ion-enhanced deposition can be modified as

$$\text{DR}_{\text{ion}} = \sum_i \sum_j \frac{K_j}{\rho_{\text{film}}} \Gamma_j s_{ij}, \tag{9}$$

where subscript i and j represent neutral and ion species, respectively.

The major positive ions in C_4F_8 plasmas considered in this study is CF_3^+ and the major fluorocarbon neutral species is CF_2.[18] Therefore, $K_i = K_j = 1$ in Eqs. (8) and (9). It is noted that the role of F atoms can be complicated: they may etch the deposited films and reduce the effective deposition rate, and they can be incorporated into the deposited films and increase the deposition rate.

C. Ion sputtering of polymer

In this work, it is assumed that the polymer film deposited on the silicon surface is consumed mainly by the ion sputtering process to induce etching. A widely used analytical formula for calculating the sputtering yields is known as the Bohdansky formula.[19] The Bohdansky formula was deduced by fitting an analytical transport model by Sigmund[20] using experimental data and appropriate scaling parameters. It describes the sputtering yield as a function of the incident ion energy at normal incidence

$$Y(E, \theta = 0^\circ) = Q S_n^{TF}(\varepsilon) \left[1 - \left(\frac{E_{\text{th}}}{E}\right)^{2/3}\right] \left(1 - \frac{E_{\text{th}}}{E}\right)^2, \tag{10}$$

where Q and $S_n^{TF}(\varepsilon)$ are known as the yield factor and the nuclear stopping cross section normalized to the reduced energy ε, respectively.[21] E_{th} is the threshold energy for sputtering.[22] For the dependence of the sputtering yield on the angle of incidence, Yamamura[23] proposed a procedure which is based on the assumption that the angular dependence can be described by a factor to the yield at normal incidence

$$Y(E, \theta) = Y(E, \theta = 0^\circ) \frac{1}{\cos^f \theta} \exp\left[f \cos \theta_{\text{opt}} \left(1 - \frac{1}{\cos \theta}\right)\right], \tag{11}$$

where for f and θ_{opt} are empirical parameters.

The physical sputtering yield of silicon in this study is assumed negligible compared to the yield of ion-enhancing

Redistribution subject to AVS license or copyright; see http://scitation.aip.org/termsconditions. Download to IP: 128.174.163.244 On: Mon, 11 Aug 2014 16:28:55

etching (5–10 at an energy of 100 eV). On the other hand, the surface binding energy for a small polymer molecule to an amorphous bulk polymer surface is expected to be much smaller than the C-C bond. A modified sputtering yield is proposed by Rauf *et al.*[24]

$$Y(E_i, \theta = 0°) = 6.88(E_i - 10)^{0.5}, \tag{12}$$

where E_i is the ion energy in eV. This sputtering yield in Eq. (12) will be used for polymer sputtering simulation throughout this study.

In this study, the TSV wafers are biased at a frequency of 400 kHz, which is significantly lower compared to the TCP power frequency (13.56 MHz). In this case, the ion energy distribution (IAD) can be characterized by a bimodal distribution with minimum and maximum energy peaks at[25]

$$E_{\min} = T_e \ln\left(\frac{1}{2\varepsilon}\right), \quad E_{\max} = T_e \ln\left(\frac{1 + e^{V/T_e}}{2\varepsilon}\right). \tag{13}$$

It can be calculated that for SF_3^+ ions, the resulting $E_{\min}$ and $E_{\max}$ are 30.7 eV and 130.7 eV at a bias voltage of 100 V, respectively.

At any location in the etch profile, the sputtering rate of the polymer film is the integral of the sputtering yield of the ion flux of all energies from all angles visible by this location

$$\text{Sputtering Rate} = \int_{E_{\min}}^{E_{\max}} \int_{\theta_{\min}}^{\theta_{\max}} \Gamma(E, \theta) Y(E, \theta) d\theta \, dE, \tag{14}$$

where $\Gamma(E, \theta)$ is the ion flux at an energy of E incident at an angle of θ. The values of $\theta_{\min}$ and $\theta_{\max}$ vary at different locations in the geometry. In the simulation model of this study, the origin of the coordinates is defined as the bottom right point of the mask on the left, as shown in Fig. 2. It is noted the y axis is defined as the opposite of the direction at which etching will take place. The normal direction n at any surface element is pointed out from the surface, defined by two normalized vectors (n_x, n_y). Figure 2 shows the case of $n_x < 0$ and $n_y < 0$ for the surface element. The angle denoted by θ_1 is therefore representing the normal direction of the surface

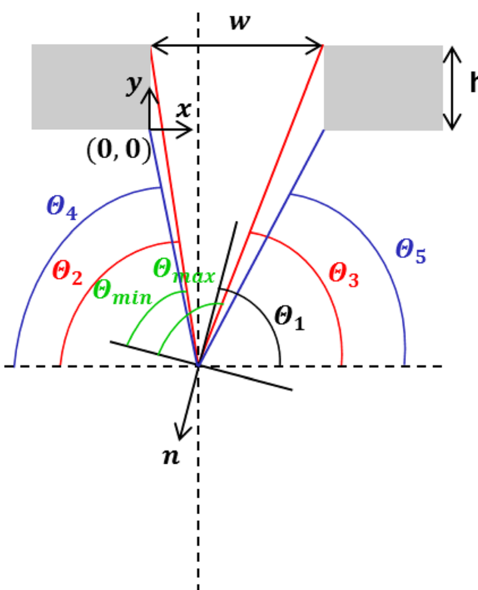

FIG. 2. (Color online) Definition of geometry and expression of a surface element in the etching model.

$$\theta_1 = \cos^{-1}(-n_x). \tag{15}$$

It is noted that angle defined by function $\cos^{-1}$ is in the range of (0, π). θ_2 and θ_4 are defined as the angles from the lines jointed by the corners of left mask and the point under consideration to the −x direction. Similarly, θ_3 and θ_5 are the angles from the lines jointed by the corners of right mask and the point under consideration to the x direction

$$\theta_2 = \tan^{-1}\left(\frac{h - y}{x}\right), \quad \text{for } x > 0, \tag{16}$$

$$\theta_3 = \tan^{-1}\left(\frac{h - y}{w - x}\right), \quad \text{for } x < w, \tag{17}$$

$$\theta_4 = \tan^{-1}\left(\frac{-y}{x}\right), \quad \text{for } x > 0, \tag{18}$$

$$\theta_5 = \tan^{-1}\left(\frac{-y}{w - x}\right), \quad \text{for } x < w. \tag{19}$$

Note that angle defined by function $\tan^{-1}$ is in the range of $(-\pi/2, \pi/2)$.

Consequently, the $\theta_{\min}$ and $\theta_{\max}$ in this case can be expressed as

$$\theta_{\min} = \theta_1 + \theta_2 - \pi/2, \tag{20}$$

$$\theta_{\max} = \theta_1 - \theta_3 + \pi/2. \tag{21}$$

Detailed geometric considerations of the polymer sputtering by ions are carried out in the Appendix by consideration different ion incident orientations. With these considerations, $\theta_{\min}$ and $\theta_{\max}$ can be written as

$$\theta_{\min} = \min\{\max[\theta_1 + \theta_2 - \pi/2,\ \theta_1 + \theta_4 - \pi/2,\ 0], \min[\theta_1 - \theta_3 + \pi/2,\ \theta_1 - \theta_5 + \pi/2,\ \pi]\}, \tag{22}$$

$$\theta_{\max} = \min[\theta_1 - \theta_3 + \pi/2,\ \theta_1 - \theta_5 + \pi/2,\ \pi]. \tag{23}$$

The angular distribution of ion flux is assumed by a Gaussian distribution function

$$\Gamma(\theta') = \Gamma(\theta' = \pi/2) \frac{1}{\sigma\sqrt{2\pi}} \exp\left[-\frac{(\theta' - \pi/2)^2}{2\sigma^2}\right], \tag{24}$$

where θ' is the angle with respect to horizontal axis. The total ion flux arrived at any location in the geometry can be calculated as

Redistribution subject to AVS license or copyright; see http://scitation.aip.org/termsconditions. Download to IP: 128.174.163.244 On: Mon, 11 Aug 2014 16:28:55

$$\Gamma_{\text{ion}} = \int_{\theta_{\min}}^{\theta_{\max}} \frac{\Gamma(\theta' = \pi/2)\frac{1}{\sigma\sqrt{2\pi}}\exp\left[-\frac{(\theta'-\pi/2)^2}{2\sigma^2}\right]\cos(\pi/2-\theta)}{\cos(\theta'-\pi/2)} d\theta, \tag{25}$$

or

$$\Gamma_{\text{ion}} = \int_{\theta_{\min}}^{\theta_{\max}} \frac{\Gamma(\theta' = \pi/2)\frac{1}{\sigma\sqrt{2\pi}}\exp\left[-\frac{(\theta-\theta_1)^2}{2\sigma^2}\right]\cos(\pi/2-\theta)}{\cos(\theta-\theta_1)} d\theta. \tag{26}$$

It is important to point out that the ion flux expression in Eq. (26) does not include the energy dependence yet. Ion energy incident at different energies may have different initial angular distributions, denoted by deviation σ, and different initial vertical flux, $\Gamma(\theta' = \pi/2) = \Gamma_0$. However, the angular dependence does not change for different energies. As a result, the total ion flux accounted for the effects of ion energies can be written as

$$\Gamma_{\text{ion}} = \int dE \int_{\theta_{\min}}^{\theta_{\max}} \times \frac{\Gamma_0(E)\frac{1}{\sigma(E)\sqrt{2\pi}}\exp\left[-\frac{(\theta-\theta_1)^2}{2\sigma^2(E)}\right]\cos(\pi/2-\theta)}{\cos(\theta-\theta_1)} d\theta. \tag{27}$$

Experiments in this study are carried out in the LAM 2300 Syndion C etching system (LAM Research). Several advantages of the Syndion C system for fabricating HAR TSV profiles are: (1) Fast switches of less than 10 ms lag are used to control the gas flow rate and duration time. The minimum during time for a single step is 100 ms. (2) Multiple etching parameters on the Syndion C control panel, such as chamber pressure, gas flow rate, and bias voltage, can be individually ramped for a Bosch or non-Bosch etching process. Eight micrometer CD TSV features with a mask thickness of 5 μm has been used for the experimental study in this work.

III. RESULTS AND DISCUSSION

A. Bosch process

The Bosch process performed for the TSV etching in this study consists of alternating SF_6 etching phases and C_4F_8 passivation phases. In a SF_6 etching phase, the overall etching process can be considered as a sequence of a polymer sputtering phase and a Si etching phase. The considerations of polymer sputtering yield at any surface in the geometry have been introduced in the previous section. In this study, a surface reaction model is integrated in COMSOL to calculate the removal rate of the polymer films during a given process time of the Si etching phase. The governing equation for the surface concentration c_s is written as

$$\frac{\partial c_s}{\partial t} = \nabla \cdot (-D\nabla c_s) + R_s, \tag{28}$$

where D is the surface diffusion coefficient, R_s [mol/(m^2·s)] is the surface reaction rate, which is the sum of surface reactions and adsorption/desorption mechanisms of all sources. In the Bosch process using C_4F_8 in the passivation phase, the deposited polymer film is normally a Teflon-like layer formed by CF_2 monomers. The sputtered monomers are therefore assumed to be CF_2 in the Bosch process simulation model. In this study, the sputtering ions taken into account in the polymer removal are the SF_3^+ ions. As a result, the surface sputtering rate of polymer monomer CF_2 can be expressed as

$$R_s = -\frac{1}{N_a}\sum_{E_{\text{ion}}}\int_{\theta_{\min}}^{\theta_{\max}} \Gamma_{SF_3^+}(E_{\text{ion}},\theta)Y(E_{\text{ion}},\theta)d\theta, \tag{29}$$

where N_a is the Avogadro constant. The density of the polymer film deposited by C_4F_8 plasma is assumed to be the same as that of Teflon (2.65×10^{22} CF_2/cm^3). In our simulation for the Bosch process, it is assumed that Si etching can take place at surface locations where the polymer film is completely removed, or

$$c_s < 0. \tag{30}$$

The methodology for simulating the Si etching by SF_6 is simply isotropic etching. For an effective Bosch process, the sidewall of the etch profile should be covered by the polymer film at all time to prevent lateral etching. This means the thickness of the polymer film on the sidewalls does not affect the etch profile if the condition $c_s > 0$ is satisfied at all sidewall locations. Therefore, the thickness of the polymer film can be treated as uniform at any geometry surface at the end of a passivation phase and can be estimated the polymer deposited at the bottom of the profile. In this study, the major depositing ions are the CF_3^+ ions ($K_{CF_3^+} = 1$) for the Bosch process, and the surface concentration of the polymer film (mol/m^2) deposited at the end of a passivation phase is

Redistribution subject to AVS license or copyright; see http://scitation.aip.org/termsconditions. Download to IP: 128.174.163.244 On: Mon, 11 Aug 2014 16:28:55

TABLE I. List of parameters in one etching/passivation cycle used in the model.

	C_4F_8 passivation phase				SF$_6$ etching phase					
	Γ ($m^{-2}s^{-1}$)	K_{ion}	t_p (s)		Γ ($m^{-2}s^{-1}$)	E (eV)	Y_{ie}	σ (°)	s	t_e (s)
CF_3^+	1.2×10^{21}	1	0.5	SF_3^+	1.0×10^{21}	200	15	3	1	0.7
				SF_3^+	1.5×10^{21}	30	5	58	1	
				F	1.77×10^{23}	N/A	N/A	N/A	0.24	

$$c_s(0) = \frac{1}{N_a} K_{CF_3^+} \Gamma_{CF_3^+} t_p = \frac{1}{N_a} \Gamma_{CF_3^+} t_p, \tag{31}$$

where t_p is the duration of the passivation phase. Therefore, the condition for the etching to occur at any surface location is

$$R_s t_e > c_s(0), \tag{32}$$

where t_e is the duration of the etching phase. In this simulation model, a loop of alternating etching and passivation phases is established as a function of time to predict the etch profile at a given time. An example etch profile calculated by this simulation model using the parameters in Table I is shown in Fig. 3.

Simulation result in Fig. 3 shows that an anisotropic profile can be achieved using the Bosch process in Table I. In this process, a neutral F flux, a high-energy ion flux, and a low-energy ion flux have been taken into account in the etching phase. High energy ions are important in etching in the polymer sputtering process. Two important phenomena can be seen from the ion flux and neutral flux distributions on the surface of the etch profile: First of all, total ion flux is larger on the sidewalls at the top and at the bottom of the etch profile than everywhere else. The high ion flux at the top sidewalls is due to the low-energy ions with large angular spread σ. The high ion flux at the bottom is because of the high line-of-sight low- and high-energy ion fluxes from the mask opening. Second of all, the neutral F flux on the sidewalls is generally decreasing as the aspect ratio increases, and the F flux at the bottom is only slightly larger than the F flux at the nearby sidewall locations. This is due to the angular spread of the neutral flux is much larger that of high-energy ions. It can be seen that the critical dimension (CD) of the etch profile is generally decreasing as the etched depth increases, which is exactly the aspect-ratio dependent etching (ARDE). It is clear from the simulation results that the cause for the ARDE is the decrease of the neutral/ion fluxes when aspect ratio is increased.

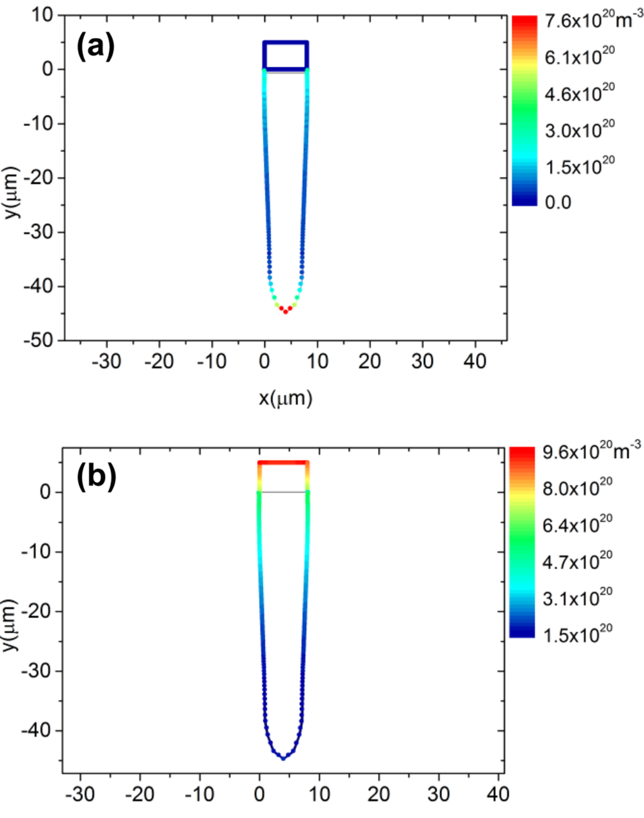

FIG. 3. (Color online) Etch profile of the simulation model etched by a Bosch process shown in Table I for a total process time of 240 s, the top box stands for the open mask for TSV features [color scale indicates (a) total ion flux and (b) neutral F flux on etch surface, respectively].

The sensitivity of the dual-energy ion model can be verified by comparing an experimental etch profile with simulation profiles realized by the single ion energy model and the dual ion energy model, respectively. Figure 4(a) showed an experimental etch profile realized by isotropic SF_6 etching, Fig. 4(b) is the best-fit simulation profile calculated by assuming all ions have the same energy (single ion energy model), and Fig. 4(c) is the best-fit simulation profile calculated by considering a high-energy ion flux and a low-energy ion flux (dual ion energy model). In both models, the number density of neutral F radicals is determined in the simulation model by matching the undercut with the experimental profile, and the ion flux and IAD angle are determined by matching the etch depth and bowing of the overall experimental profile, respectively.

It can be clearly seen from the comparison between Figs. 4(a) and 4(b) that although the undercut and bowing of the simulation profile is matched at the same etch depth with the experimental profile, the sharper bottom observed in the experimental profile cannot be predicted by the single ion energy model. On the other hand, a better match of the experimental etch profile is achieved by the simulation model by taking into account a high- and a low-energy ion flux with a ratio of 1:20, as shown in Fig. 4(c). The reason for the better match of the dual ion energy model with the experimental profile is because two ion energy distribution is

Redistribution subject to AVS license or copyright; see http://scitation.aip.org/termsconditions. Download to IP: 128.174.163.244 On: Mon, 11 Aug 2014 16:28:55

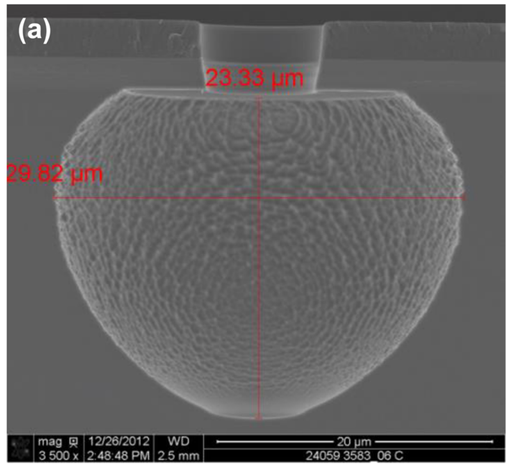

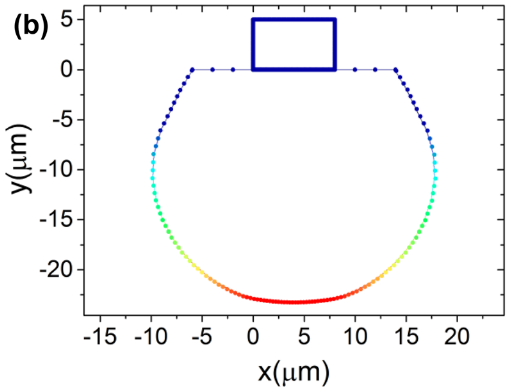

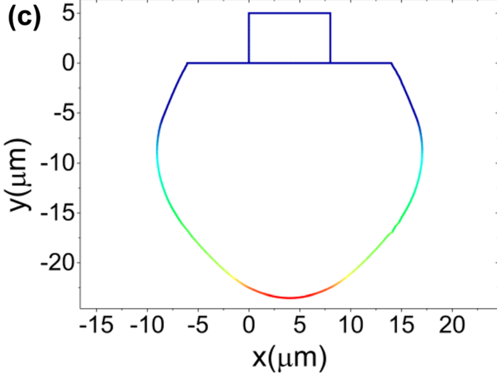

FIG. 4. (Color online) Comparison of (a) an experimental Si etch profile as a result of SF_6 isotropic etching, (b) simulation etch profile realized by a single ion energy model, the best match is obtained when SF_3^+ ion flux $\Gamma_0 = 2.14 \times 10^{22}\,m^{-2}\,s^{-1}$ and angular spread $\sigma = \tan^{-1}$(mask.with/mask.height $\approx 58°$), and neutral F etching ($\Gamma_F = 1.36 \times 10^{25}\,m^{-2}\,s^{-1}$, s = 0.24), and (c) simulation profile realized by assuming a high-energy SF_3^+ ion flux ($Y_{ie} = 9.7$, $\Gamma_0 = 1.04 \times 10^{20}\,m^{-2}\,s^{-1}$, $\sigma = 6°$), a low-energy SF_3^+ ion flux ($Y_{ie} = 5.0$, $\Gamma_0 = 3.0 \times 10^{21}\,m^{-2}\,s^{-1}$, $\sigma = $ atan(mask.width/mask.height) $\approx 58°$), and neutral F atom flux ($\Gamma_F = 1.36 \times 10^{25}\,m^{-2}\,s^{-1}$, $s = 0.24$).

closer to the bimodal IAD behavior in a bias-pulsing situation, and the high-energy ions with smaller angular distribution and large Y_{ie} account for the sharp tip at the bottom of the experimental profile.

One of the most characteristic phenomenon of the etch profiles etched by a Bosch process is the scallop-shaped sidewalls. A detailed graph showing the sidewalls underneath the mask of the etch profile in Fig. 3 is shown again in

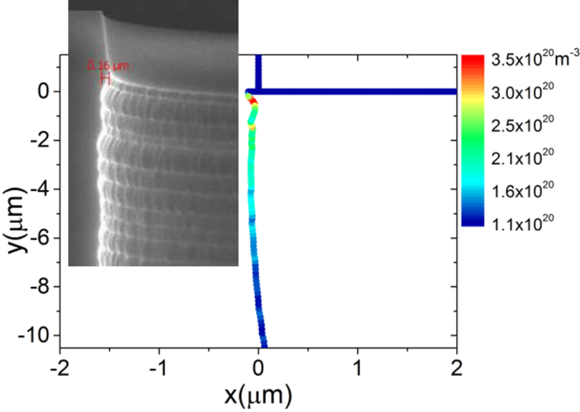

FIG. 5. (Color online) Detailed graph showing the sidewalls of the etch profile underneath the mask (color scale indicates the total ion flux on Si surface).

Fig. 5. It can be seen that the ion flux is not continuously increased or decreased along the etch direction, instead it increases and decreases in cycles, which is an indication for the small scalloped profile, especially for the first few etching/passivation circles. The reason for this behavior is that the high ion flux at the top of the etch profile quickly removes the polymer layer and induces lateral etching but the polymer removal process becomes slower as etch depth increases due to insufficient ion bombardment. This has

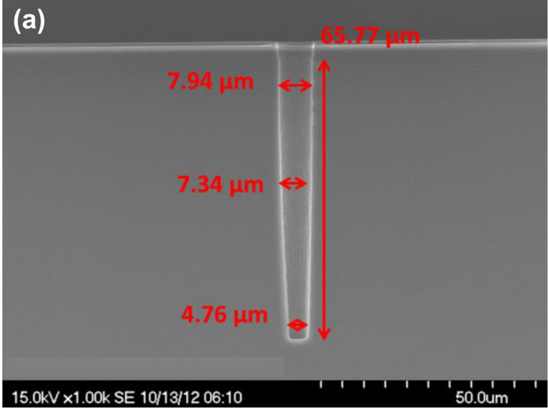

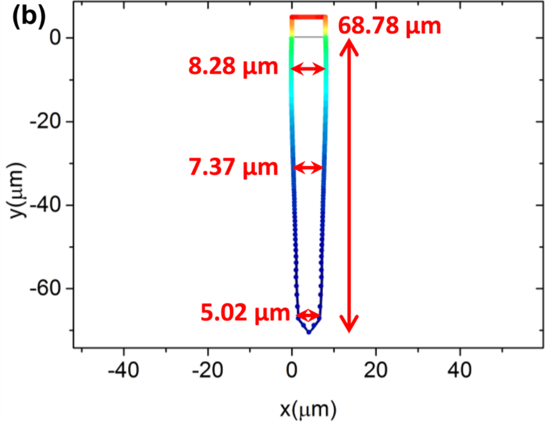

FIG. 6. (Color online) Comparison of (a) experimental etch profile and (b) simulation result for the baseline Bosch process.

Redistribution subject to AVS license or copyright; see http://scitation.aip.org/termsconditions. Download to IP: 128.174.163.244 On: Mon, 11 Aug 2014 16:28:55

TABLE II. Variables used in the simulation model for the baseline Bosch process.

C_4F_8 passivation phase				SF$_6$ etching phase						
	Γ ($m^{-2}s^{-1}$)	K_{ion}	t_p (s)		Γ ($m^{-2}s^{-1}$)	E (eV)	Y_{ie}	σ (°)	s	t_e (s)
CF_3^+	1.2×10^{21}	1	0.5	SF_3^+	1.0×10^{21}	230	15	1.74	1	0.7
				SF_3^+	1.5×10^{21}	30	5	58.0	1	
				F	1.36×10^{25}	N/A	N/A	N/A	0.24	

been shown in a typical experimental TSV profile, as compared in Fig. 5.

For a typical Bosch process, the etch profile calculated by the simulation model has the best match with the experimental profile by calibrating the flux of the SF_3^+ and CF_3^+ ions with ER and CDs at TSV top, middle, and bottom, as shown in Fig. 6. These parameters are listed in Table II.

It can be seen from Fig. 6 that the simulation profile and experimental profiles show similar morphology. The predicted profile have slightly larger etch depth and CD compared to the experimental profile, indicating that the surface concentration of the passivation polymer is slightly underestimated in the simulation model in Table II. This is probably because there are polymerizing ions other than CF_3^+ can be dissociated from a C_4F_8 plasma and participate in the polymerization process.

The parameter ramping simulation can be easily integrated into the model established for the Bosch process in this study. It has been discussed that modifications on some experimental parameters, such as pressure and bias voltage, can result in changes of multiple variables in the simulation model. This correspondence has been shown in Table III. The quantitative relation between an experiment parameter and its corresponding variables is obtained from experimental data from our plasma chemistry study or theoretical calculations from other references. As an example, we studied the effect of the bias voltage ramping in the Bosch process by simulation. It is assumed in the model that the bias voltage V_b mainly affects the angular distribution of ions. The time dependence of the angular spread σ of SF_3^+ ions

$$\sigma_{ion} = \tan^{-1}\left(\frac{\sqrt{0.026\,\mathrm{eV}}}{\sqrt{E_{ion}} - \sqrt{0.026\,\mathrm{eV}}}\right), \tag{33}$$

where E_{ion} is the ion energy bombarding at the surface. It is assumed that the ion energy of SF_3^+ is a linear function of the total process time t. The resulting $\sigma(t)$ is plotted in Fig. 7 when V_b is ramped down from 200 V to 130 in 360 s. It can be clearly seen that the half-with of ions increases with time but not linearly. The resulting simulation profile is compared with the experimental profile in Fig. 8.

TABLE III. List of parameters in a single-step etching process used in the model ($\Gamma_F = 1.36\times10^{24}$ $m^{-2}s^{-1}$).

C_4F_8 species				SF$_6$ species				
	Γ ($m^{-2}s^{-1}$)	K	σ (°)		Γ ($m^{-2}s^{-1}$)	E (eV)	Y_{ie}	σ (°)
CF_3^+	1.7×10^{22}	1	1	SF_3^+	1.0×10^{21}	130	9.7	1
CF_2	1.7×10^{21}	1	N/A	SF_3^+	1.5×10^{21}	30	5	58

B. Single-step etching process

The complexity of the single-step etching rises from interactions of the etching and passivation species. On the other hand, whether an etching particle or a passivation particle reaches at a surface location is random in the single-step etching process. For simulation purposes, it is well known that a Monte-Carlo approach is most straightforward for modeling random processes. For the finite-element analysis (FEA) simulation employed in this study, an alternative approach needs to be appropriately used for the surface chemistry mechanism.

The polymer deposition and sputtering mechanisms are expressed using the surface reaction model in the single-step etching simulation. Two deposition sources are considered in this study, a CF_3^+ ion source and a neutral CF_2 source. The overall deposition rate (DR) is therefore the sum of equations neutral and ion-assisted deposition, or

$$\mathrm{DR} = \frac{1}{N_a}\left(\Gamma_{CF_2}s_{CF_2} + \int_{\theta_{min}}^{\theta_{max}}\Gamma_{CF_3^+}(\theta)d\theta\right), \tag{34}$$

where the unit of DR is mol/m^2·s. Here, the neutral CF_2 deposition is considered uniform at all surface locations. Similarly, the polymer removal rate (sputtering rate, SR) at any surface location is determined by the energy, sputtering yield, and flux of SF_3^+ ions of all energies at all incident angles

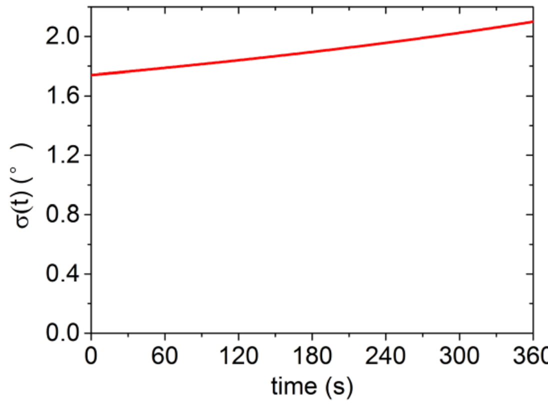

FIG. 7. (Color online) Time dependence of the angular spread of SF_3^+ ions when V_b is linearly ramped down from 200 V to 130 V in 360 s.

Redistribution subject to AVS license or copyright; see http://scitation.aip.org/termsconditions. Download to IP: 128.174.163.244 On: Mon, 11 Aug 2014 16:28:55

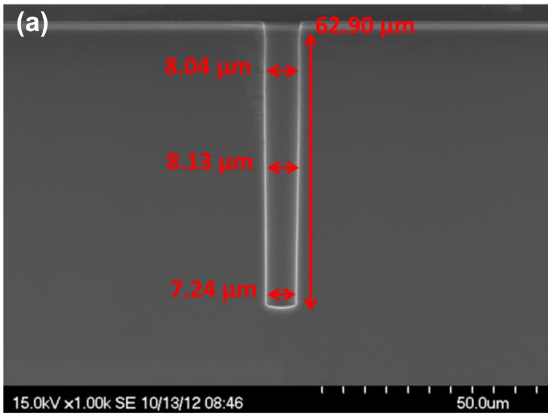

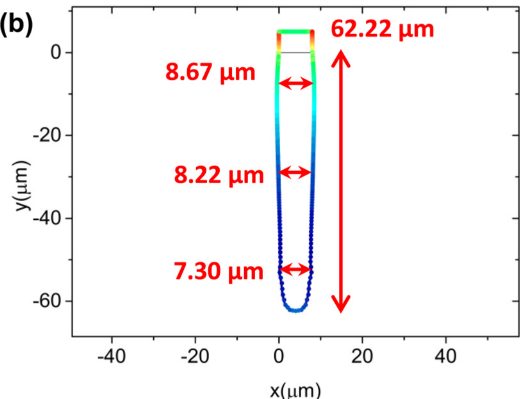

FIG. 8. (Color online) Comparison of (a) experimental etch profile and (b) simulation result for a bias ramping Bosch process.

$$\mathrm{SR} = \frac{1}{N_a}\sum_E \int_{\theta_{\min}}^{\theta_{\max}} \Gamma_{\mathrm{SF}_3^+}(E,\theta)Y(E,\theta)d\theta, \tag{35}$$

where

$$Y(E,\theta) = Y(E)Y(\theta) = 6.88\sqrt{E\ \ (\mathrm{eV}) - 10}\cdot Y(\theta), \tag{36}$$

using the expression in Eq. (12). Therefore, it can be assumed that the possibility for the etching to occur at the surface is depending on the polymer surface concentration c_s can be calculated by equation

$$\frac{\partial c_s}{\partial t} = R_s = \mathrm{DR} - \mathrm{SR}. \tag{37}$$

It is noted that c_s is calculated by adding up the effects of etching species and the deposition species arriving at a surface location at the same time. This is problematic because in reality a surface location can only be occupied by one particle at the same time. However, the calculated surface concentration can be considered as an indicator of the polymer coverage possibility at this surface location. As a result, the surface reaction velocity (deformation velocity) will decrease if the surface coverage possibility of polymer is large. For the single-step etching simulation, the deformation velocity is assumed to follow an exponential function at locations covered by a polymer film

$$v_n = \begin{cases} (\mathrm{ER_{th}} + \mathrm{ER_{ie}}) \times b\left[\exp\left(-\frac{c_s}{a}\right)\right], & \text{for } c_s > 0 \\ (\mathrm{ER_{th}} + \mathrm{ER_{ie}}), & \text{for } c_s < 0 \end{cases}, \tag{38}$$

where $\mathrm{ER_{th}}$ and $\mathrm{ER_{ie}}$ are the thermal etch rate by F atoms and ion-enhanced etch rate by SF_3^+ ions. b and a are empirical coefficients determined by the properties of polymer and indicates passivation ability of the deposited film. The maximum value of b is 1. It can be seen that if the value of a is chosen to satisfy $a \gg c_s$ for surface locations which are more likely covered by polymer films ($c_s > 0$), the surface reaction velocity v_n is weakly depending on c_s since $exp(-c_s/a) \to 1$. For surface locations not covered ($c_s < 0$) by a polymer film, v_n is assumed to be the overall etching velocity by neutrals and ions. Simulated etch profiles produced by the single-step etching process listed in Table III are compared at different empirical parameter a in Fig. 9.

It is stated in Eq. (38) that different values of a only affect locations with surface concentration $c_s > 0$. As it can be seen in Fig. 8, these surface locations are created at the top bowing of the etch profile. The surface reaction velocity v_n is increased when a smaller value of a is chosen, resulting in a larger bowing in the etch profile. In this case, the difference of the widest CD in the etch profiles when a is chosen as 1000 and 10 is less than 0.1%, thus dependence of etch profile on the value of a is not significant. The formation of

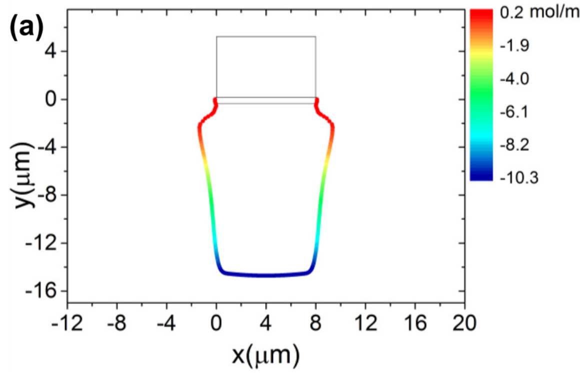

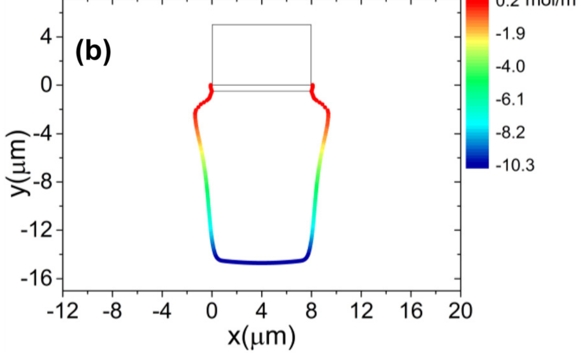

FIG. 9. (Color online) Simulation etch profile of the single-step etching shown in Table III when the empirical parameter a is (a) 1000 and (b) 10, for a total etch time of 60 s and $b = 1$ (color scale indicates the surface polymer concentration c_s).

Redistribution subject to AVS license or copyright; see http://scitation.aip.org/termsconditions. Download to IP: 128.174.163.244 On: Mon, 11 Aug 2014 16:28:55

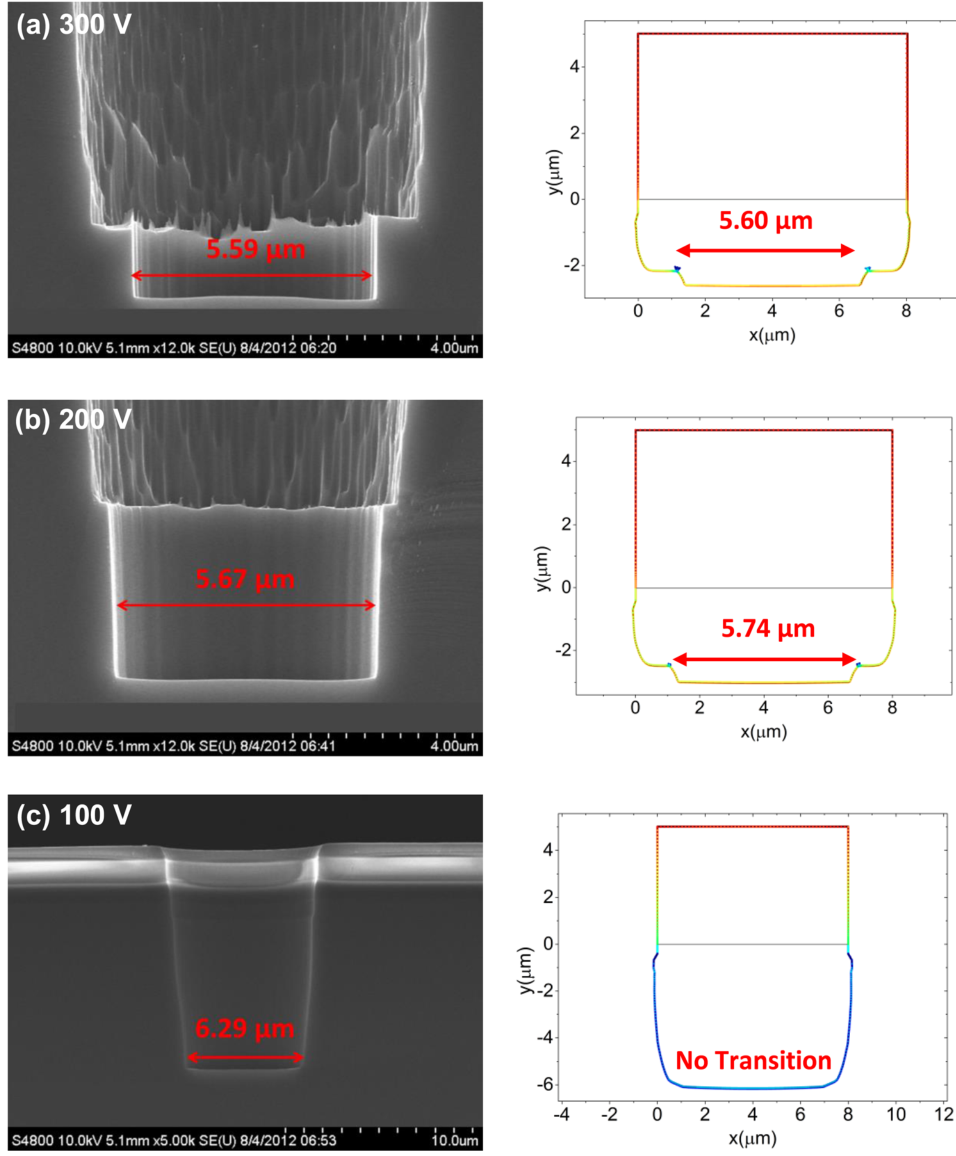

FIG. 10. (Color online) Comparison of the transitions in the experimental TSV profiles and calculated by the simulation model at a V_b of (a) 300 V, (b) 200 V, and (c) 100 V.

the bowing shape at the top of the etch profile is owing to the large-angle SF_3^+ ion bombardment on the weaker passivation sidewalls, which is strongly depending on the angular spread σ and the flux of SF_3^+ and CF_3^+ ions. These parameters are considered as variables in the etching simulation models throughout this study so that the significance of each parameter can be compared and investigated.

As shown in Fig. 10, a transition can be formed on the TSV profile using the single-step etching method, especially when the bias voltage V_b is large and the SF_6 flow rate is high. This phenomenon can be well explained by the simulation model. Using the deformation velocity in Eq. (38), the appearance positions of the transition formed at the bottom of the TSV profiles as a function of bias voltage V_b are investigated. Parameters used in the simulation is corresponding to an experimental condition of a gas flow rate of 200/200 sccm SF_6/C_4F_8 and a pressure of 60 mTorr. For the three major ions species considered in the model (high-energy SF_3^+ ions, low-energy SF_3^+ ions, and CF_3^+ ions), the angular spreads σ's used to best match the transition location at a V_b of 100 V, 200 V, and 300 V are listed in Table IV, and the resulting formation of the transition computed by the model is compared with the experimental profiles in Fig. 10.

It can be speculated that the inherent reason for the formation of the transition is the discontinuity in the etching/passivation chemistry when the ratio of etching and passivation varies at different surface locations. This ratio can be expressed by the polymer surface concentration c_s in the simulation model

TABLE IV. List of angular spread σ for the ion species considered in a single-step etching processes at different V_b's [$\Gamma_F = 1.36\times10^{24}\,m^{-2}s^{-1}$, $\Gamma_{SF_3^+}(\text{high } E) = 2.5\times10^{20}\,m^{-2}s^{-1}$, $\Gamma_{SF_3^+}(\text{low } E) = 6\times10^{21}\,m^{-2}s^{-1}$, $\Gamma_{CF_3^+} = 1.7\times10^{23}\,m^{-2}s^{-1}$, $\Gamma_{CF_2} = 1.1\times10^{22}\,m^{-2}s^{-1}$].

V_b (V)	CF_3^+	SF_3^+ (high E)	SF_3^+ (low E)
100	86.8°	2.34°	43.0°
200	61.0°	1.74°	26.0°
300	50.0°	1.44°	23.5°

Redistribution subject to AVS license or copyright; see http://scitation.aip.org/termsconditions. Download to IP: 128.174.163.244 On: Mon, 11 Aug 2014 16:28:55

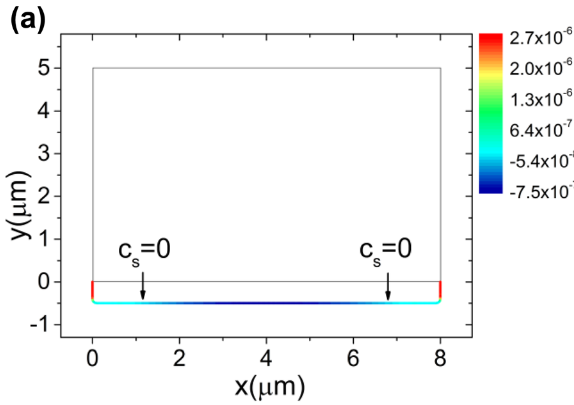

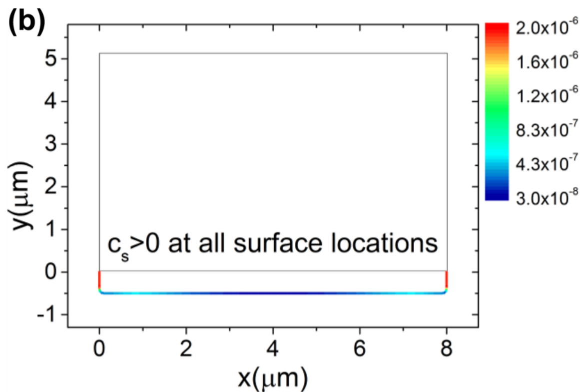

FIG. 11. (Color online) Initial c_s distribution at a V_b of (a) 200 V and (b) 100 V. The transition will be formed at the two positions where c_s is 0 at 200 V. However, no transition will be formed at 100 V because the initial values of c_s is larger than 0 at all surface locations.

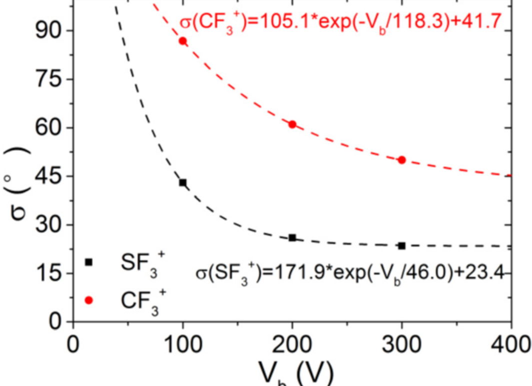

FIG. 12. (Color online) Fit functions for angular spread σ of the low-energy SF_3^+ and CF_3^+ ions.

for the single-step etching. As it is stated previously, the value of c_s indicates of the possibility of surface reaction and therefore determines the surface etching velocity. More importantly, the phenomenon that multiple transitions can be formed on the TSV profile indicate that a multisegment surface reaction function in terms of the polymer surface concentration, c_s.

It can be seen from Fig. 10 that both of the experimental results and the simulation model predicted that a transition is formed at the bottom of the TSV profile at a V_b of 200 V and 300 V, but no transition is formed at 100 V. The CD of the TSV below the transition calculated by the simulation is in good agreement with the experimental results using the parameters in Table IV. The reason for the transition formed at a certain position is that the c_s values of the two sides (left and right) with respect to this position fall into different regimes in Eq. (38); thus, a discontinuity appears in the etching profile due to different surface reaction velocities. The inherent cause of the c_s difference is the competition between the polymer-sputtering ions (SF_3^+) and the polymer-depositing ions (CF_3^+) at different surface locations due to their different ion angular distributions. The initial c_s distributions at a V_b of 200 V and 100 V are shown in Fig. 11. A comparison of the simulation profile in Figs. 10(b) and 11 clearly shows that the transition is initially formed at the locations where the value of c_s becomes 0 and will involve with time.

Previous section has described the inherent mechanism for the transition formation on the TSV profiles produced by the single-step etching method. It is important to point out that of all angular spread parameters in Table IV, only the angular spread of the high-energy SF_3^+ ions is obtained from theoretical calculation using Eq. (33), other angular spreads, including the angular spreads of the low-energy SF_3^+ ions and CF_3^+ ions, are obtained by matching the simulation results to the experimental profiles. In this study, a general criterion of validating the value of assumed angular spread σ is that the value of σ should decrease when V_b is increased. With the σ values obtained in Table IV, the best-fit functions can be found for the low-energy SF_3^+ ions and the CF_3^+ ions, respectively. These functions are shown in Fig. 12. Combined with Eq. (33), a complete set of equations for all ions species considered in the single-step etching model is listed in Eq. (39). The equation set expresses the relation between the angular spread σ and the bias voltage V_b. Therefore, they can be used to estimate the σ value at any other V_b within a reasonable range.

$$\sigma(^\circ) = \begin{cases} \tan^{-1}\left(\dfrac{\sqrt{0.2}}{\sqrt{E_{ion}(V)} - \sqrt{0.2}}\right), & \text{for high } E \text{ SF}_3^+ \text{ ions} \\ 171.9 \times \exp\left(-\dfrac{V_b(V)}{46.0}\right) + 23.4, & \text{for low } E \text{ SF}_3^+ \text{ ions} \\ 105.1 \times \exp\left(-\dfrac{V_b(V)}{118.3}\right) + 41.7, & \text{for CF}_3^+ \text{ ions} \end{cases} \quad (39)$$

Redistribution subject to AVS license or copyright; see http://scitation.aip.org/termsconditions. Download to IP: 128.174.163.244 On: Mon, 11 Aug 2014 16:28:55

Using Eq. (39), TSV etch profiles produced by the single-step etching method can be predicted. Since the bias voltage V_b and the SF_6 flux are the two most important factors for the formation transition, the effects of V_b and SF_6 flux will be studied with the simulation model individually. It is expected that the threshold bias voltage for forming the transition is between 100 and 200 V. Therefore, it will be interesting to see whether a transition can be formed or not at a V_b of 150 V. On the other hand, in order to test the applicable range of the established simulation model, a simulation profile using the V_b values beyond 300 V is necessary. As a result, the simulation profiles at a V_b of 150 V and 350 V are computed using the established single-step etching model, as shown in Fig. 13. The simulation model is then compared with the experimental profiles, as shown in Fig. 14.

Compare the simulation results and the experimental profiles, it can be seen that several important trends has been successfully predicted by the simulation model. First, it is predicted by the simulation that the transition is formed at a V_b as low as 150 V, as can be seen in both Figs. 13(a) and 14(a). Second, the simulation model successfully predicted the position at the bottom of the TSV profile where the transition is formed for both bias voltages. It is predicted by the simulation model that the CD of the TSV profile decreases when V_b is increased from 150 V to 350 V, which agrees well with the experiments. Lastly, it is shown in the simulation profile that the transition step in the etch profile is small at a V_b of 150 V due to the CD decrease as etch depth increases. However, a sharper transition step is clearly seen at a V_b of 350 V in the simulation profile. The same trend has been observed from the experimental profiles in the overall profiles shown in Fig. 14. It is noticed that the slope of the sidewalls above the transition is larger (meaning less vertical sidewalls) when a smaller V_b (150 V) is applied. Since the only variables modified in the simulation model at different bias voltages are the ion angular spreads, it can be concluded that the sidewall incline (CD decrease) at a small V_b is caused by the larger ion angular spreads of all ion species.

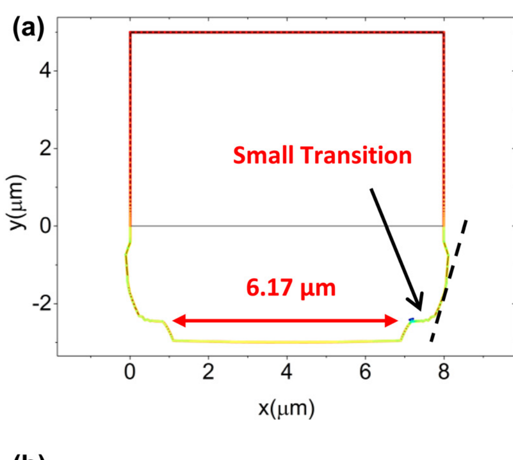

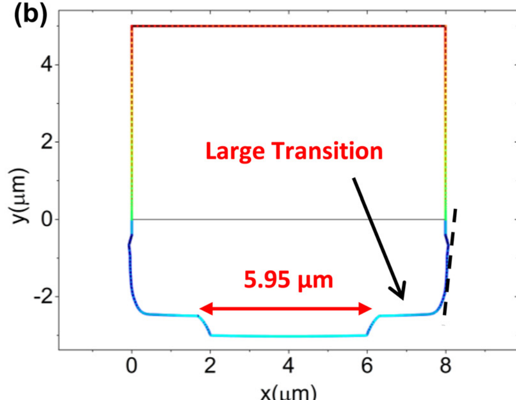

FIG. 13. (Color online) Prediction of the TSV etch profiles by the simulation model at a V_b of (a) 150 V and (b) 350 V using the angular spread σ calculated by Eq. (39).

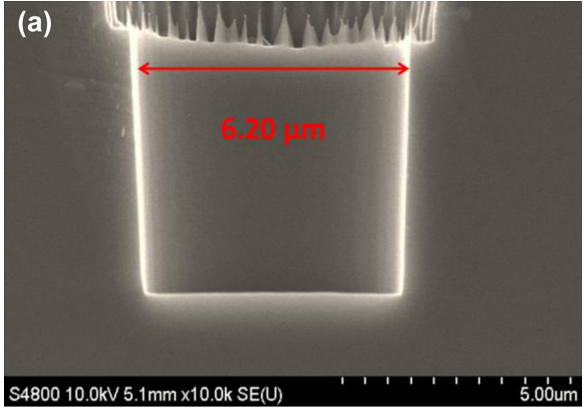

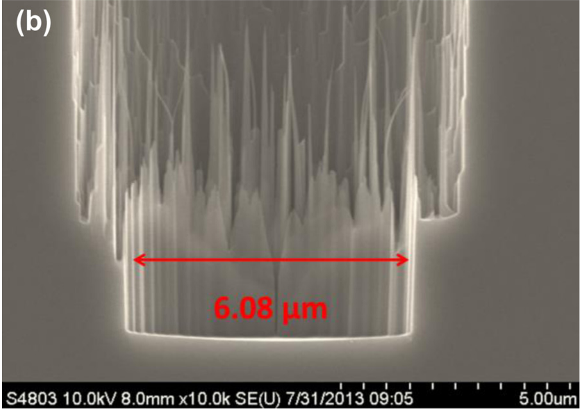

FIG. 14. (Color online) Experimental TSV profiles produced at a V_b of (a) 150 V and (b) 350 V, as compared to the simulation profiles in Fig. 12.

IV. CONCLUSION

The simulation models established based on the FEA method for TSV etching can be applied to different etching processes in this study. Etch profile prediction is possible for Bosch process and single-step etching by the established simulation models assuming appropriate etching mechanisms, including fluxes of neutral species and ions, angular distribution of ions, and ion energy. In reality, the overall effect of each experimental parameter on the etching processes results from collective effects of individual ion fluxes and neutral fluxes in the plasma. Therefore, the effect of different ion fluxes and neutral fluxes cannot be differentiated from a specific etch profile produced by an experimental process alone.

One of the major advantages of the Bosch process model established in this study is it is capable of modeling the

Redistribution subject to AVS license or copyright; see http://scitation.aip.org/termsconditions. Download to IP: 128.174.163.244 On: Mon, 11 Aug 2014 16:28:55

TABLE V. Experimental parameters and their corresponding variables in the simulation models.

Experimental parameters	Corresponding variables of simulation models (subscript "ion" represents SF_3^+ and CF_3^+ ions)		
Pressure	Γ_{ion}	Γ_F	σ_{ion}
SF_6 flow	$\Gamma_{SF_3^+}$	Γ_F	
C_4F_8 flow	$\Gamma_{CF_3^+}$	Γ_{CF_2}	
Bias voltage	σ_{ion}	E_{ion}	
Temperature	ER_{th}		
TCP power	Γ_{ion}	Γ_F	

parameter ramping process by integrating time-dependent process parameters. Since the process window of the Bosch process is narrow, the simulation model can be a cost-effective way of predicting TSV profiles. The comparison between the single-step etching simulation results and experiments shows that the underlying reason for the formation of the transition is the discrepancy of ion angular distributions of etching species and depositing species. Observations from both experiments and simulation indicate that low-energy SF_3^+ ions do not significantly introduce lateral etching on the sidewalls and the bottom of the TSV profile, and the TSV etching is mainly induced by the high-energy SF_3^+ ions.

Table V lists the important parameters of the experimental processes for the TSV etching and their corresponding variables used in the simulation models.

It is important to point out that some other profile-defining variables are depending on the value(s) of one or multiple variables listed in Table V in the simulation, for example, the silicon etching yield Y_{ie} is a function of E_{ion}, the integrated ion flux and polymer sputtering yield at a surface location is a function of Γ_{ion}, E_{ion}, and σ_{ion}. Therefore, the information obtained from the distributions of these variables at different conditions can also be used to understand the etching mechanisms from the simulation models.

ACKNOWLEDGMENTS

This work was supported by Micron Technology, Inc. The authors would like to thank the dry etch group for great support and discussion.

APPENDIX

1. Geometric considerations for polymer ion sputtering

Other than the case shown in Fig. 2, other possible situations of orientations of a surface element when its normal vector n is in other quadrants of the coordinates are shown in Fig. 15. The value of θ_1 is defined in this model as the following:

$$\theta_1 = \begin{cases} \cos^{-1}(-n_x), & \text{if } n_y < 0 \\ -\cos^{-1}(-n_x), & \text{if } n_y > 0 \text{ and } n_x < 0 \\ \pi + \cos^{-1}(-n_x), & \text{if } n_y > 0 \text{ and } n_x > 0 \end{cases}, \quad \text{(A1)}$$

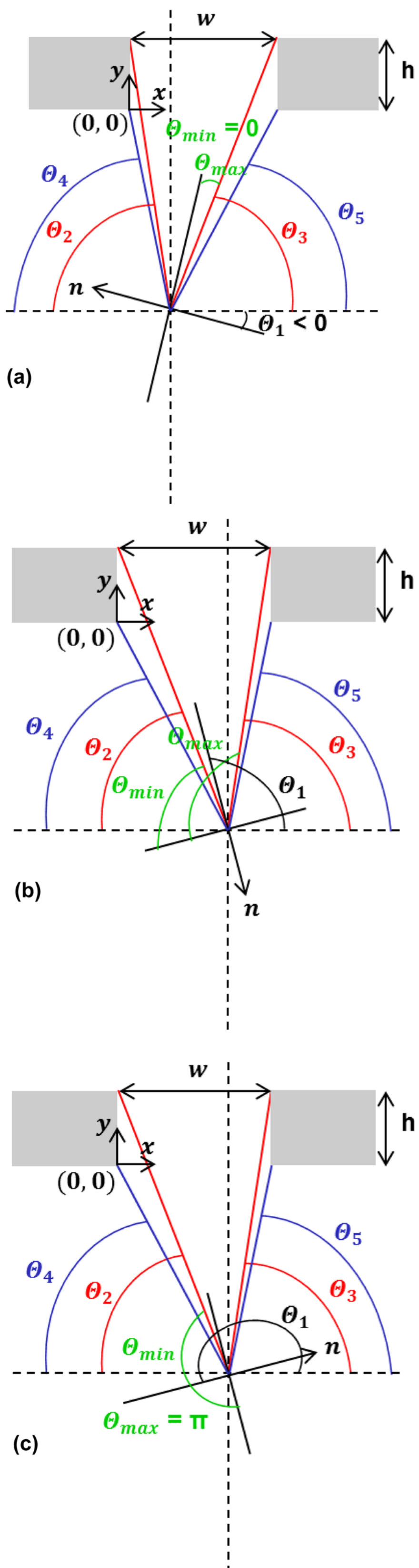

FIG. 15. (Color online) Angle definition of θ_1 for different surface orientations.

so that the expressions for θ_{min} and θ_{max} remains the same as in Eqs. (20) and (21). However, the values of θ_{min} and θ_{max} go to 0 and π when incident flux is shadowed by the surface; thus, Eqs. (20) and (21) can be modified as

Redistribution subject to AVS license or copyright; see http://scitation.aip.org/termsconditions. Download to IP: 128.174.163.244 On: Mon, 11 Aug 2014 16:28:55

$$\theta_{min} = \max\ [\theta_1 + \theta_2 - \pi/2,\ 0], \tag{A2}$$

$$\theta_{max} = \min\ [\theta_1 - \theta_3 + \pi/2,\ \pi]. \tag{A3}$$

Similar considerations need to be carried out for angles used in the etch geometry other than θ_1. Figure 16 shows the situation when the flux is partially or completely shadowed by the mask. In the case of the value of θ_2, θ_3, θ_4, or θ_5 larger than $\pi/2$, they are redefined as

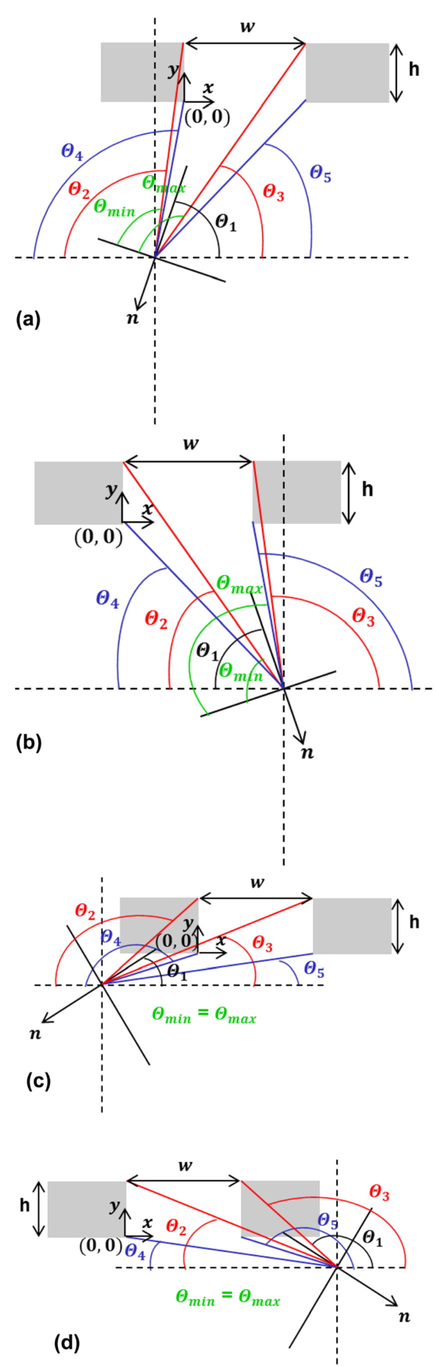

FIG. 16. (Color online) Geometry diagrams for locations where flux is [(a) and (b)] partially and [(c) and (d)] completely shadowed by the mask.

$$\theta_2 = \pi + \tan^{-1}\left(\frac{h-y}{x}\right), \quad \text{for } x < 0, \tag{A4}$$

$$\theta_3 = \pi + \tan^{-1}\left(\frac{h-y}{w-x}\right), \quad \text{for } x > w, \tag{A5}$$

$$\theta_4 = \pi + \tan^{-1}\left(\frac{-y}{x}\right), \quad \text{for } x < 0, \tag{A6}$$

$$\theta_5 = \pi + \tan^{-1}\left(\frac{-y}{w-x}\right), \quad \text{for } x > w. \tag{A7}$$

Equations (16)–(19) together with Eqs. (A4)–(A7) complete the definitions for θ_2-θ_5.

With these considerations, θ_{min} and θ_{max} can be written as

$$\theta_{min} = \min\ \{\max\ [\theta_1 + \theta_2 - \pi/2,\ \theta_1 + \theta_4 - \pi/2, 0],\ \min\ [\theta_1 - \theta_3 + \pi/2,\ \theta_1 - \theta_5 + \pi/2,\ \pi]\}, \tag{A8}$$

$$\theta_{max} = \min\ [\theta_1 - \theta_3 + \pi/2,\ \theta_1 - \theta_5 + \pi/2,\ \pi]. \tag{A9}$$

[1]J. U. Knickerbocker *et al.*, IEEE J. Solid-State Circuits **41**, 1718 (2006).
[2]F. Laermer and A. Schilp, U.S. Patent 5,501,893, 26 March 1996.
[3]H. Rhee, H. Kwon, C. K. Kim, H. J. Kim, J. Yoo, and Y. W. Kim, J. Vac. Sci. Technol. B **26**, 576 (2008).
[4]A. A. Ayón, R. Braff, C. C. Lin, H. H. Sawin, and M. A. Schmidt, J. Electrochem. Soc. **146**, 339 (1999).
[5]A. Summanwar, F. Neuilly, and T. Bourouina, "Research in microelectronics and electronics," Ph.D. dissertation, 22–25 June 2008 (IEEE, Istanbul, Turkey, 2008), pp. 129.
[6]Y -J. Hung, S -L. Lee, B. J. Thibeault, and L. A. Coldren, IEEE J. Sel. Topics Quantum Electron. **17**, 869 (2011).
[7]U. Gerlach-Meyer, Surf. Sci. **103**, 524 (1981).
[8]D. L. Flamm, V. M. Donnelly, and J. A. Mucha, J. Appl. Phys. **52**, 3633 (1981).
[9]D. C. Gray, I. Tepermeister, and H. H. Sawin, J. Vac. Sci. Technol. B **11**, 1243 (1993).
[10]C. Steinbruchel, Appl. Phys. Lett. **55**, 1960 (1989).
[11]J. P. Chang, J. C. Arnold, G. C. H. Zau, H.-S. Shin, and H. H. Sawin, J. Vac. Sci. Technol. A **15**, 1853 (1997).
[12]S. A. Vitale, H. Chae, and H. H. Sawin, J. Vac. Sci. Technol. A **19**, 2197 (2001).
[13]R. Foest, J. K. Olthoff, R. J. VanBrunt, E. C. Benck, and J. R. Roberts, Phys. Rev. E **54,** 1876 (1996).
[14]W. Möller and W. Eckstein, Nucl. Instrum. Meth. B **2**, 814 (1984).
[15]J. F. Ziegler, J. P. Biersack, and U. Littmark, *Stopping Powers and Ranges in All Elements* (Pergamon, New York, 1985), Vol. 1.
[16]A. Milella, F. Palumbo, P. Favia, G. Cicala, and R. d'Agostino, Plasma Process. Polym. **1**, 164 (2004).
[17]I. R. Saraf, M. J. Goeckner, B. E. Goodlin, K. H. R. Kirmse, C. T. Nelson, and L. J. Overzet, J. Vac. Sci. Technol. B **31**, 011208 (2013).
[18]A. V. Vasenkov, X. Li, G. S. Oehrlein, and M. J. Kushner, J. Vac. Sci. Technol. A **22**, 511 (2004).
[19]J. Bohdansky, Nucl. Instrum. Meth. B **2**, 587 (1984).
[20]P. Sigmund, Phys. Rev. **184**, 383 (1969).
[21]N. Matsunami, Y. Yamamura, Y. Itakawa, N. Itoh, Y. Kazumata, S. Myagawa, K. Morita, and R. Shimizu, Rad. Eff. Lett. **57**, 15 (1981).
[22]J. Bohdansky, J. Roth, and H. L. Bay, J. Appl. Phys. **51**, 2861 (1980).
[23]Y. Yamamura, Y. Itikawa, and N. Itoh, *Angular Dependence of Sputtering Yields of Monatomic Solids* (Research Information Center, Institute of Plasma Physics, Nagoya University, Japan, 1983).
[24]S. Rauf, W. Dauksher, S. Clemens, and K. Smith, J. Vac. Sci. Technol. A **20**, 1177 (2002).
[25]F. F. Chen and J. P. Chang, *Lecture Notes on Principles of Plasma Processing* (Springer, New York, 2003).

Redistribution subject to AVS license or copyright; see http://scitation.aip.org/termsconditions. Download to IP: 128.174.163.244 On: Mon, 11 Aug 2014 16:28:55